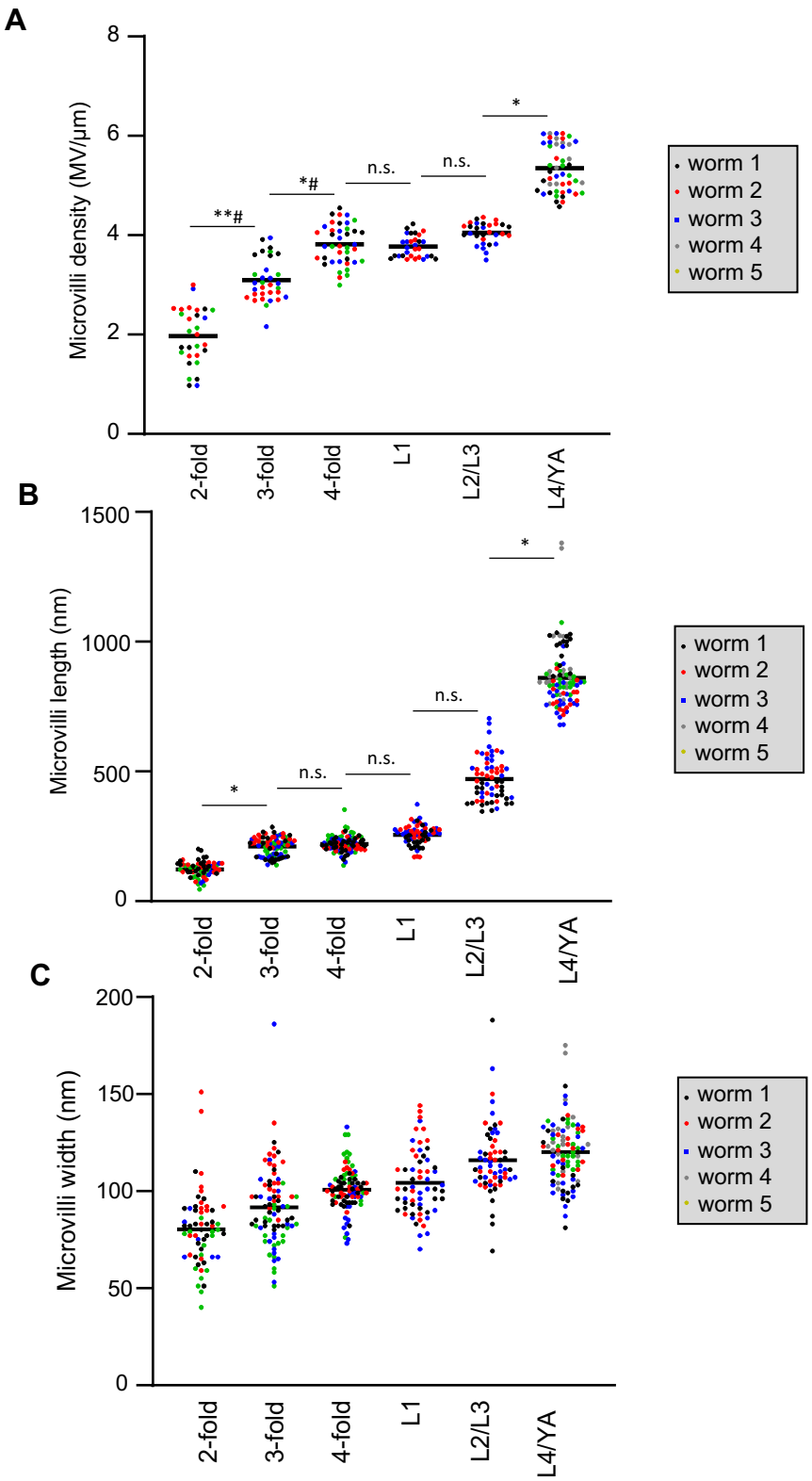

Fig. S1. Individual values of brush border measurements by TEM, related to Fig. 1.
Colorized dots represent individual worms at the indicated developmental stages. Bar is the grand mean of all the measurements. Microvilli density was measured on 3-13 slices/worm, microvilli length and width on 6-29 microvilli/worm. N.s., non-significant, *p<0,05, **p<0,01. Except in A, where some data were analysed by unpaired t-test (#), statistical significance was calculated using Mann-Whitney test.

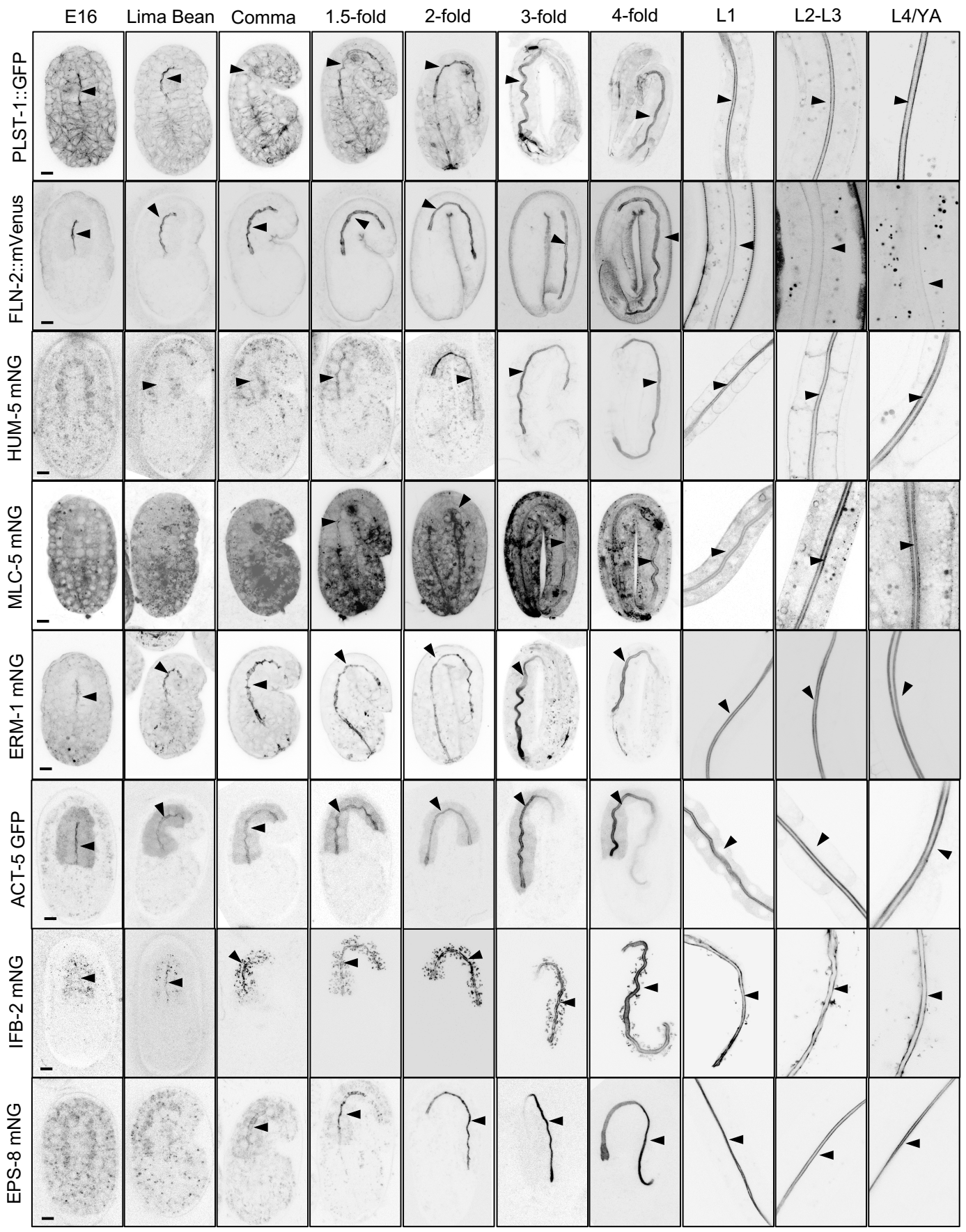

Fig. S2. Systematic analysis of brush border markers during *C. elegans* development. Representative confocal images of the endogenously tagged markers indicated (except ACT-5::GFP). Arrowheads show the intestinal cells apical PM. Scale bar is 5 µm.

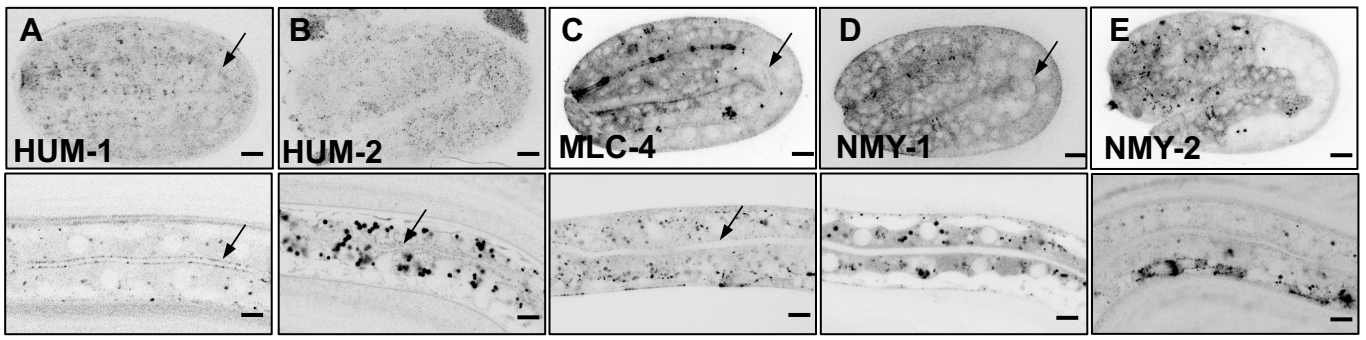

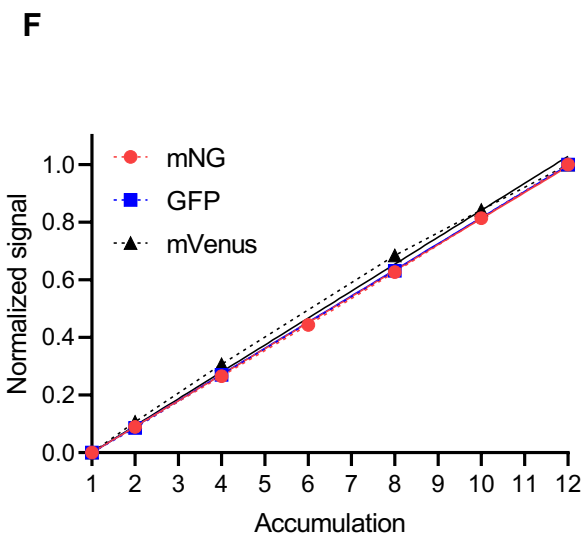

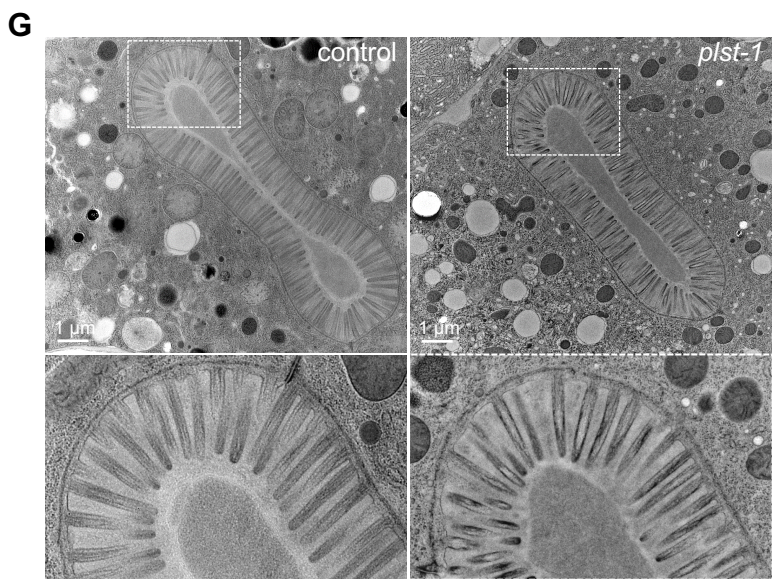

Fig. S3. Systematic analysis of brush border markers during *C. elegans* development.
(A-E) Representative confocal images of *C. elegans* strains expressing endogenously tagged versions of the indicated markers, which showed no apical accumulation during *C. elegans* intestine development. Scale bar, 5 µm. (F) Control of the quantitative assessment of brush border markers arrival at the apical PM. Accumulation of IFB-2::mNG, PLST-1::GFP and FLN-2::mVenus signal linearly increases with image accumulation. Experimental points are linked by dashed lines, bold lines show simple linear regression curve fitting. n=1-2 measurement per timepoint for each fluorophore. (G) Representative TEM images of control (N2) and *plst-1(tm4255)* L4/young adult worms (N=3 worms in each condition).

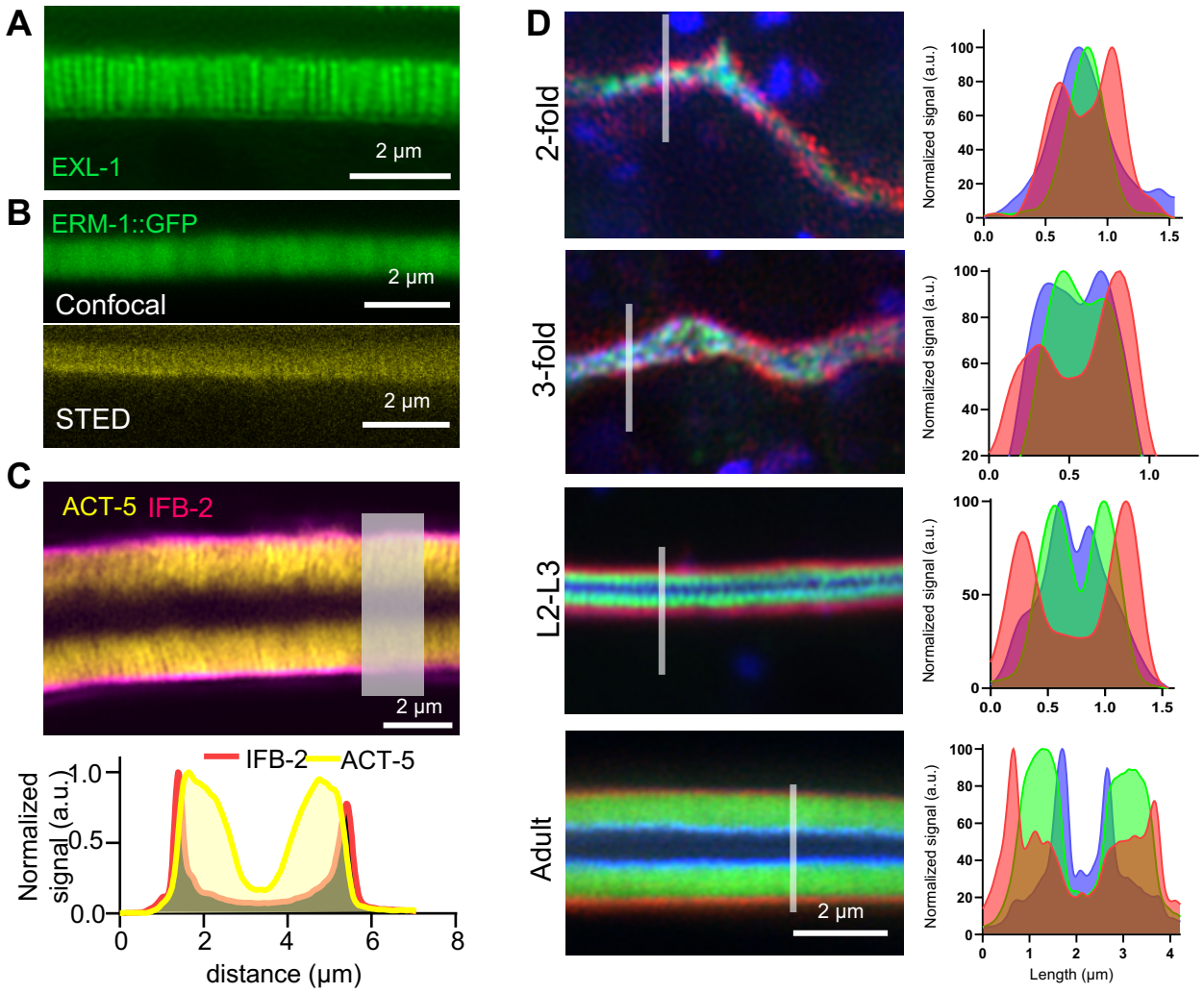

Fig. S4. Super-resolution imaging of brush border markers *in vivo*. (A) Representative super-resolution image of exogenously expressed EXL-1::GFP. (B) ERM-1::GFP was imaged in adult worms using the indicated microscopes. (C) Super-resolution images of a *C. elegans* adults co-expressing ACT-5::GFP and IFB-2::wSc. Bottom panel shows a normalized intensity profile along the line depicted in grey. (D) Representative images of the localization of endogenously tagged EPS-8::BFP, ERM-1::mNG and IFB-2::wSc in *C. elegans* at the indicated developmental stages. Right panels show an intensity profile of the three markers along the line depicted in left panels. Scale bars, 2 µm.

.

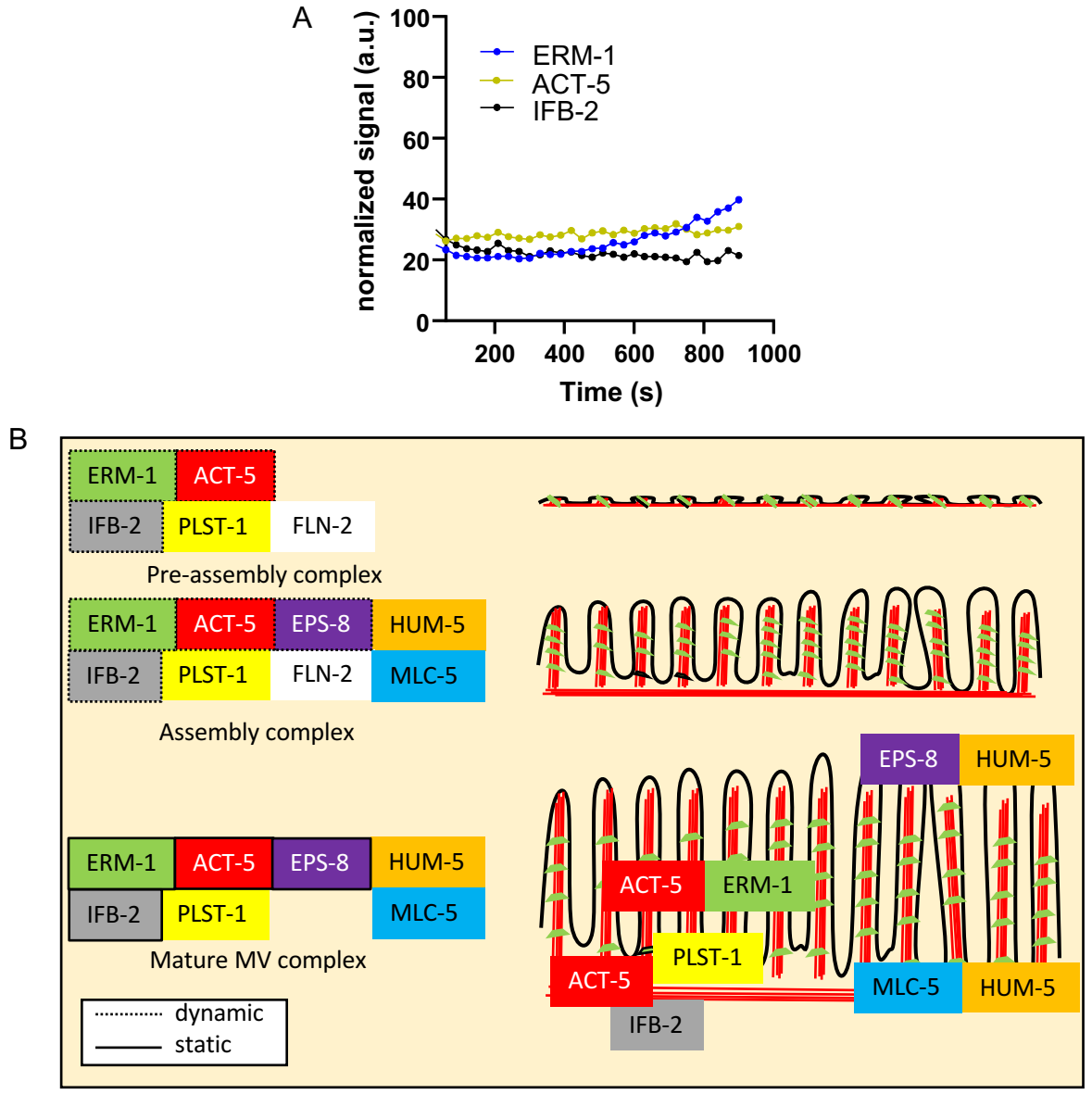

Fig. S5. Dynamic recruitment of brush border components.

(A) Longer measurement of brush border components dynamics in adult worms. The curves show the recovery of ERM-1::mNG, IFB-2::mNG and ACT-5::GFP signal every 30 s after photobleaching, measured for an extended time, n=1 for each marker. (B) Model of brush border assembly *in vivo* in *C. elegans*. Microvilli are built from a preformed *pre-assembly complex* and grow through the dynamic recruitment of brush border components, which become highly stable in the mature brush border.

Table S1. *C. elegans* strains used in this study.

Strain	Markers/targets	Genotype	Reference
FBR96	MLC-4	mlc-4(jme04[mlc-4::eGFP+loxP]) III	Francois Robin lab
FBR140	MLC-5	mlc-5(jme09[GFP^3xFLAG::mlc-5]) III	Francois Robin lab
FBR222	FLN-2	fln-2(jme-19[fln-2::mVenus]) X	Francois Robin lab
FL274	ERM-1, IFB-2	erm-1(bab59[erm-1::mNG^SEC^3xFlag]) I ; ifb-2(bab142[ifb-2::wSc]) II	Bidaud-Meynard et al., 2019
FL290	EPS-8	eps-8(bab140[eps-8::mNG]) IV	This study
FL369	ERM-1, ACT-5	fgEx13[perm-1::erm-1::gfp + rol-6 (su1006)] ; jyIs17 [vha-6p::mcherry::act-5, ttx-3p::RFP]	Bidaud-Meynard et al., 2019
FL378	ERM-1	erm-1(bab59[erm-1::mNG^3xFlag]) I	Bidaud-Meynard et al., 2019
FL379	ERM-1	bab64[erm-1::wrmSc^3xFlag] I	Bidaud-Meynard et al., 2019
FL381	ACT-5, IFB-2	fgEx12 (act-5p::act-5::gfp); ifb-2(bab142[ifb-2::wrmSc]) II	This study
FL383	EPS-8, ERM-1, IFB-2	eps-8(bab140[eps-8::mNG]) IV ; erm-1(bab59[erm-1::mNG^SEC^3xFlag]) I; ifb-2(bab142[ifb-2::wSc]) II	This study
FL384	ERM-1	erm-1(bab167[erm-1::degron-tagBFP2]) I	This study
FL385	IFB-2	ifb-2(bab153[ifb-2::mNG]) II	This study
FL386	ERM-1, PLST1	erm-1(bab167[erm-1::degron-tagBFP2]) ; plst-1(msn190[plst-1::gfp]) IV	This study
FL387	ERM1, HUM5	erm-1(bab167[erm-1::degron-tagBFP2]) ; hum-5(bab189[hum-5::mNG]) III	This study
FL388	ERM-1, MLC5	erm-1(bab167[erm-1::degron-tagBFP2]) ; mlc-5(jme09[GFP^3xFLAG::mlc-5]) III	This study
FL586	ERM-1, FLN-2	erm-1(bab167[erm-1::degron-tagBFP2]), fln-2(jme-19[fln-2::mVenus]) X	This study
LP162	NMY-2	nmy-2(cp13[nmy-2::GFP + LoxP]) I	CGC
LP462	MRCK-1	mrck-1(cp189[mrck-1::GFP::3xFlag]) V	CGC
MCP111	PGP-1	pgp-1(bab111[mNG^3xFlag::pgp-1]) IV	Bidaud-Meynard et al., 2019
MCP184	HUM-2	hum-2(bab184[hum-2::mNG]) V	This study
MCP189	HUM-5	hum-5(bab189[hum-5::mNG]) III	This study
MCP223	EXL-1	exl-1(bab223[exl-1::mNG]) II	This study
ML2540	NMY-1	nmy-1(mc82[nmy-1::gfp]) X.	Vuong-Brender et al., 2017
OH2211	EXL-1	otEx1184 [exl-1p::exl-1::GFP + rol-6(su1006)]	CGC
QQ226	HUM-1	hum-1(cv21[hum-1::RFP]) I	CGC
RZB213	PLST-1	plst-1(msn190[plst-1::gfp]) IV	Ding et al., 2017
RZB365	PLST-1	plst-1(tm4255)	Ronen Zaidel-Bar lab
VJ268	ACT-5	fgEx12(act-5p::act-5::gfp)	Zhang et al., 2012

File S1.

Click here to download Supplementary File 1